Solar wind, F10.7, and geomagnetic activity relationship to the equatorial plasma mass density at geosynchronous orbit

V. Veibell, R.S. Weigel, and R.E. Denton

September 7, 2016

Abstract

We consider two types of events, identified by decreases in D_{st} below a threshold value and increases in the the equatorial mass density at geosynchronous altitudes, ρ_{eq}, above a threshold value using the *Takahashi et al.* [2010] dataset. From the D_{st} events and 1-day averages, we find that there is a statistically weak and small-amplitude difference between ρ_{eq} on the day of the event and the days before and after. When hourly averages are considered, a significant peak is found to occur six hours after event onset, and the primary factor that determines the post-onset peak amplitude in ρ_{eq} is elevated $F10.7$. In addition, for hourly averages, ρ_{eq} following the onset of a D_{st} event depends on the north-south component of the interplanetary magnetic field, B_z after the time of onset, with higher average B_z four hours after the event onset corresponding to larger ρ_{eq} value 7-11 hours after onset. From the ρ_{eq} events, we find a weak dependence on B_z after the onset of an event, with higher average B_z four hours after the event onset corresponding to larger ρ_{eq} values 24-36 hours after onset.

1   Introduction

20

21   The dependence of the plasmapause location on geomagnetic activity was observed as early

22   as *Carpenter* [1966] and there are well–validated models of the plasmapause location as

23   a function of L, MLT, and geomagnetic activity (*Lemaire* [1998], *Moldwin et al.* [2002],

24   *O'Brien and Moldwin* [2003]). Models also exist for the plasmasphere density (*Gallagher*

25   *et al.* [1988]; *Lemaire* [1998]) with similar parameterization.

26   The dependence of the plasma density outside of the nominal plasmapause location on

27   geomagnetic and solar wind conditions has not been extensively studied until the past decade

28   (*Takahashi et al.* [2006]; *Takahashi et al.* [2010]; *Denton et al.* [2016]). Earlier works that

29   considered profiles of ion density found a significant dependence of the plasmapause location

30   on geomagnetic activity (*Chappell et al.* [1970]; *Maynard and Grebowsky* [1977]; *Carpenter*

31   *and Anderson* [1992]), but the relationship between geomagnetic activity and density outside

32   of the plasmapause was not explicitly considered.

33   *Takahashi et al.* [2006] estimated magnetospheric mass density using measurements from

34   the CRRES satellite during a 73-day period in 1991 when CRRES was in an elliptical, near

35   equatorial orbit and primarily beyond the nominal plasmapause. They found that the local

36   average ion mass, M, had some correlation with geomagnetic activity, with more negative

37   hourly D_{st} values corresponding to higher M and larger 1.5- and 3-day averages of K_p

38   corresponding to higher M (3-hour averages of K_p had little visual correlation with M).

39   The mass density estimates were obtained from CRRES observations in the MLT range of

40   [12:00, 18:00] with most observations at L between 5 and 7 R_E.

41   *Denton et al.* [2006] found a weak relationship between D_{st} and K_p and the field line

42   distribution of plasma mass density, ρ, using observations of the first three toroidal Alfvén

43   harmonic frequencies for L in the range of 6-8 R_E. A more pronounced peak in the distri-

44   bution along a field line near the equator was found for lower D_{st} and larger K_p, but the

45   equatorial value of ρ was found to be similar for D_{st} bins of [-142, -31] and [-31, 37] nT and

46   K_p bins of [1.5,3.4] and [3.4, 5.9].

47 *Takahashi et al.* [2010] developed a mass density dataset using measurements from the

48 Space Environment Monitor instruments on the Geostationary Operational Environmental

49 Satellites (GOES) satellites from 1980 through 1992, with most measurements in the range

50 of $L = 6.8 \pm 0.2 R_E$. The mass density was estimated using the the Alfvén wave velocity

51 relationship, $V_A = B/\sqrt{\mu_0 \rho}$, a magnetic field model, and a numerical solution to a wave

52 equation with an ionospheric boundary and the assumption of a zero resistance ionosphere.

53 The equatorial mass density, ρ_{eq}, was derived from the estimated mass density using a

54 power law dependence on the geocentric distance to the field line of the observation, R,

55 $\rho = \rho_{eq}(LR_E/R)^{1/2}$. They found a high correlation (~ 0.94) between 27-day averages of

56 $F10.7$ and 27-day medians of ρ_{eq}.

57 *Takahashi et al.* [2010] noted that downward drops in the D_{st} index coincided with sig-

58 nificant changes in ρ_{eq} for L near 6.8 R_E. For five storms, two had ρ_{eq} increases after D_{st}

59 minimum, two had ρ_{eq} spikes before the minimum, and one showed little change in ρ_{eq}. A

60 key result was that when daily-averaged measurements were considered, the epoch average

61 of D_{st} for storms with a minimum $D_{st} < -50$ nT showed an enhancement in ρ_{eq} the same

62 day as minimum D_{st} in the epoch averages.

63 *Yao et al.* [2008] studied the relationship between D_{st} and the number density of low-

64 energy O^+ in different regions (ring current and plasma sheet) using the TEAMS and ESA

65 instruments on the low-altitude and high-inclination orbiting FAST satellite and found that

66 the average N_{O+} across the sampled L-shells (2-14) had a strong correlation (0.88) with the

67 minimum D_{st} of the storm. Although the correlation at geosynchronous distances was not

68 calculated, the data presented for four events show that the enhancements in N_{O+} tended

69 to appear near D_{st} minimum ($\pm$ 2 hours).

70 The above results indicate that (1) the mass density at geosynchronous distances is best

71 correlated with $F10.7$ and (2) there exists a much weaker statistical relationship between

72 mass density and the geomagnetic activity indices K_p and D_{st}. In this work we consider the

73 dependence of mass density estimates in the *Takahashi et al.* [2010] data set and attempt

74 to identify and statistically characterize the relationship between geomagnetic activity with

75 mass density at geosynchronous distances. In addition, we attempt to identify solar wind

76 variables that may drive or be associated with the changes.

2 Data Preparation and Overview

78 The parameters ρ_{eq} and $F_{10.7}$ are from the dataset of *Takahashi et al.* [2010] data are available

79 from 1980 through 1991 from GOES 2, 3, 5, 6 and 7. All other parameters used are from

80 *Kondrashov et al.* [2014], which has coverage from 1972 through 2013 and are on a 1–hour

81 time grid. ρ_{eq} is the inferred equatorial mass density based on the 3rd harmonic torodial

82 frequency of magnetic field measurements as described in *Takahashi et al.* [2010]. The

83 smallest cadence for ρ_{eq} values is 10 minutes. To compute an hourly median over the same

84 interval for which the solar wind parameters were averaged, the median of all ρ_{eq} values in

85 a given hour window was used. GOES 6 had the longest span of available (May 1983 to

86 August 1991) data and the primary results presented are for GOES 6 while measurements

87 from other satellites were used for consistency checks.

88   The top panel of Figure 2 shows the long-term trends of $\log_{10}(\rho_{eq})$ from GOES 6 and

89 $F_{10.7}$ computed using the median values in 27-day non-overlapping windows. A scatter plot

90 of these two lines is shown in the lower panel of Figure 2 along with that for 1–day and

91 1–hour medians. The linear correlation for GOES 6 using all measurements is found to

92 be 0.94, which is the same value documented by *Takahashi et al.* [2010] who used combined

93 measurements from all satellites in the time interval of 1980 through 1991 using the constraint

94 $06:00 \leq MLT \leq 12:00$, $K_{p3d} \geq 1.0$ and $D_{st} \geq -50$ nT. Our 27-day correlations for GOES

95 2, 5, and 7 are 0.81, 0.78, and 0.87, and the time range of coverage of measurements from

96 these satellites is 1980-01-01/1983-05-16, 1983-01-01/1987-02-28, and 1983-05-27/1991-08-

97 29, respectively.

3 Results

Two types of events are considered. The first is a drop in the D_{st} index below the threshold value of -50 nT. These types of events are considered in order to determine if there is a well-defined ρ_{eq} dependence on geomagnetic activity as indicated by the D_{st} index. It is expected that the plasmasphere will exhibit two responses near the time of these threshold crossings. First is the movement of the plasmapause earthward (*Lemaire* [1998]) and the second is a possible change in density due to magnetospheric processes.

The second type of event is an increase in ρ_{eq} above a threshold of 20 amu/cm^3. It is expected that some of these increases will typically occur after a period of quiet geomagnetic activity. In this case, the plasmapause boundary may move outward past geosynchronous orbit and the increase will be due to measurements being made inside the plasmapause. A second possible reason for the increase could be due to the same mechanism associated with increases that occur during enhanced geomagnetic activity.

3.1 D_{st} Events

Our first analysis uses GOES-6 data only from the time interval 1989-1991, which corresponds to the interval used in the epoch analysis of *Takahashi et al.* [2010]. In this interval, there were 75 D_{st} events where D_{st} remained below the -50 nT threshold for at least 12 hours. Only events with an onset time between 06:00 and 12:00 MLT were considered. The first hour of a local minimum in D_{st} following a threshold crossing defines the zero epoch time, and for each event, $4 \cdot 24$ hours were considered before and $8 \cdot 24$ hours after onset. For multiple detected threshold crossings within 24 hours of each other, the first crossing was selected as the event onset because visual inspection showed the subsequent crossings to typically be from brief downward deviations during the recovery period of a geomagnetic storm. To compute the epoch averages on a daily time scale, the median value of all available measurements for all events centered on a window of ± 12 hours of the epoch zero hour was computed, and these

123   averaging windows were shifted in increments of 24 hours. Similar results are obtained if we

124   first reduce each event time series to have a 1-day cadence by computing medians for each

125   event in 1-day bins and then compute the medians across the averaged event time series on

126   each epoch day.

127   The stack plot in the upper panel of Figure 3 shows the epoch averages for the 75 events

128   from 1989-1991 using data from GOES 6. The minimum D_{st} median is -75 nT. Consistent

129   with *Takahashi et al.* [2010], D_{st} events correspond to elevated ρ_{eq} on the day of the event

130   relative to the day before and after, although the magnitude of increase observed here is 4.5

131   amu/cm^3 instead of the increase of $\sim$10 amu/cm^3 found in Figure 11 of *Takahashi et al.*

132   [2010]. The vertical green bars in the ρ_{eq} plot show the number of ρ_{eq} values that were used

133   to compute the medians and red error lines. The uncertainty is shown with error lines for

134   each parameter that have a width that is twice the standard deviation of the values used in

135   computing the median divided by the square root of the number of values. For the non-ρ_{eq}

136   parameters, the number of measurements used in computing the medians is typically equal

137   to the number of events, which is much larger than the number of ρ_{eq} values as all available

138   measurements were used instead of restricting to only values where a ρ_{eq} value also existed.

139   In the lower panel of Figure 3, it is shown that the trends seen in the analysis of 1989-

140   1991 also hold for the entire span of measurements from GOES 6 (with coverage years of

141   1983-1991) - a small elevation on the day of the event relative to the day before and day

142   after, with median averages after the day of the event being slightly lower than that before.

143   A similar result is obtained for GOES 7 (1987-1991); the result is much less significant for

144   GOES 5 (1983-1987) and is much more significant for GOES 2 (1981-1983). This trend has

145   a relationship with the average value of F10.7 during each respective coverage period, with

146   the most significance found during the 1981-1983 time interval when F10.7 was consistently

147   elevated.

148   To determine if the magnitude of the density medians in the top panel of Figure 3 on

149   epoch days -1, 0, and 1 are statistically different from each other, we used a two-population

Days	Difference (amu/cm^3)	%
-1 0	-4.48	10.90% ≥ 0
-1 1	-1.46	34.30% ≥ 0
1 0	-3.02	21.50% ≥ 0

Table 1: Results of test on of medians of ρ_{eq} shown in the top panel of Figure 3 between days of threshold crossing near (day = 1 or -1) or on the day of a D_{st} event (day = 0).

150 bootstrap test. A bootstrap sample of the medians for each epoch day was created by

151 sampling all values (with replacement) used to compute the median on each epoch day.

152 The observed difference between the medians is shown in Table 1 along with the fraction of

153 observations in 1000 bootstrap differences with a different sign than that observed.

154   If a statistically significant difference in the medians between two days existed, the frac-

155 tion of bootstrap samples with a different sign is expected to be much smaller ($< 5\%$). In

156 terms of a hypothesis test, we cannot reject the null hypothesis that the medians are the

157 same with a confidence higher than 100 minus the percentage value shown in the table; the

158 highest confidence level of 86% is in the difference between days -1 and 0.

159   A similar hypothesis test run for the bottom panel of Figure 3 yields a maximum con-

160 fidence level of $\sim$85%. For verification, the significance values were also tested using a

161 Wilcoxon rank-sum test and were found to be similar.

162   These tests indicate that there is not a statistically significant difference in medians of

163 daily-averaged ρ_{eq} on the day before and day after a threshold crossing in D_{st}. In addition,

164 the observed differences are on the order of only 20% of the value of ρ_{eq} on the onset day,

165 which is similar to the magnitude of variation in the observations over the displayed epoch

166 time interval.

167   We have also considered hourly averages of data for the events shown in the bottom panel

168 of Figure 3, which are shown in the top panel of Figure 4. In the time period of elevated

169 mass density within 6 hours of the start of the event, there are only $\sim$4 samples per hourly

170 interval and the peak value of $\sim$70 amu/cm^3 is associated with a single observation.

171   To increase the number of events, we have removed the constraint that the events must

172 occur in the MLT range of 06:00-12:00 and the constraint that D_{st} remained below the

173 threshold value for 12 hours or longer. The result is shown in the bottom panel of Figure 4.

174 The two variations from a baseline (one downwards before onset and one upwards after

175 onset) were tested for significant deviation from two baselines, one 24-12 hours before onset,

176 one 16-48 hours after onset. The probability of the downward variation coming from the

177 same distribution as the data from the left baseline is 1.06%, whereas the probability of the

178 right upward variation coming from the same distribution of the data for the right baseline

179 is 0.17%. This significant result is also maintained for GOES 2, 5, and 7. This indicates

180 that there are statistically significant variations in ρ_{eq} within 6 hours of onset when hourly

181 averages are considered. The signficance of the upward variation result is consistent with

182 previous observations of large mass density increases in the plasma trough region during

183 large geomagnetic storms (*Yao et al.* [2008]; *Takahashi et al.* [2010]).

184   To determine if there is an IMF B_z dependence, the epoch curves in the bottom panel

185 of Figure 4 for ρ_{eq} and B_z were separated into two parts based on the median value of B_z

186 within a window. One window covered the four hours before onset and onset and the other

187 covered onset and the following four hours; the result is shown in Figure 5. Any statistically

188 significant difference at a 95% confidence level between the two parts is indicated by a green

189 dot on the horizontal axis using a Wilcoxon rank-sum test. For the case where the separation

190 is made according to the value of B_z after onset, there is a visible and significant separation

191 between the curves from 7-11 hours after onset, with more negative B_z values corresponding

192 to lower values of ρ_{eq}.

193   The process for creating Figure 5 was repeated except using the sort variable $F10.7$

194 instead of B_z, and the result is shown in Figure 6. The difference between the epoch curves

195 is statistically significant at all times, as expected due to the high correlation between ρ_{eq} and

196 $F10.7$, but elevated $F10.7$ is associated with a peak in the ρ_{eq} curve approximately 5 hours

197 after onset. The values contributing to the peak were compared to a baseline of all values

198 16-48 hours after onset via a Wilcoxon rank-sum test and were found to have significantly

199 different medians at the 99% confidence level. This indicates the possibility that there must

200 be a high pre-existing baseline level of ρ_{eq} in order for an increase in ρ_{eq} to be observed for

201 a D_{st} event. This result is also consistent with the the analysis of Figure 3 when repeated

202 using measurements from GOES satellites taken during different parts of the solar cycle;

203 the significance of the differences between the days around onset were largest when the

204 measurements were taken during time intervals when F10.7 was consistently elevated.

3.2 ρ_{eq} Events

206 An alternative type of event can be defined that corresponds to large increases in ρ_{eq}. Figure 7

207 shows the epoch time series for events in which an increase of ρ_{eq} above 20 amu/cm^2 defines

208 the start of the event. In finding ρ_{eq} events, missing values were replaced with linearly

209 interpolated values. These events are associated with on-average positive B_z and small

210 values of D_{st} with little variability. Approximately 12 hours after onset, ρ_{eq} slowly decays

211 over 36 hours to near pre–onset levels.

212   Figure 7 can be compared with Figure 9 of *Denton et al.* [2016], which shows daily

213 averages of ρ_{eq} from this dataset after the onset of quiet K_p intervals. The growth shown

214 here (using the ρ_m threshold criteria with no constraint on K_p) is approximately linear and

215 lasts $\sim$ 12–18 hours whereas the 10 K_p events (elevated K_p followed by 2 days with $K_p \leq 1^+$)

216 considered by *Denton et al.* [2016] showed growth that lasted for at least 48 hours.

217   Figure 8 shows the the events of Figure 7 when separated by B_z in the same manner as

218 Figure 5. The largest difference occurs when the separation is performed after onset, with

219 more positive B_z leading to a larger peak in ρ_{eq} than more negative B_z. The rate of change

220 of ρ_{eq} also appears to be insensitive to the time windows used to determine the separation

221 (before or after onset).

222   Figure 9 shows how the epoch average curve of ρ_{eq} in Figure 7 depends on $F10.7$. Statisti-

223 cally significant differences occur independent of whether the separating factor is the average

224 of $F10.7$ before or after onset, as expected because the cadence of $F10.7$ is one day and its

225 time scale of variation is longer than that of ρ_{eq}. Events with high $F10.7$ are associated with

226 higher ρ_{eq} before and after event onset but similar peak values. As was the case for B_z, there

227 is an approximately 12–hour time span of linear growth of ρ_{eq} near the time of onset but

228 because the initial starting ρ_{eq} is higher for high $F10.7$, the associated growth rate is lower,

229 consistent with *Denton et al.* [2016].

230 ## 3.3 Summary and Conclusions

231 In recent years, various works have considered the influence of solar wind control and the

232 geomagnetic activity relationship to the equatorial plasma mass density at geosynchronous

233 orbit, generally using event studies and linear correlations (*Takahashi et al.* [2006]; *Denton*

234 *et al.* [2006]; *Yao et al.* [2008]; *Takahashi et al.* [2010]; *Denton et al.* [2011]; *Denton et al.*

235 [2016]). The event studies show a possible relationship between ρ_{eq} and solar wind and

236 geomagnetic activity indicators such as K_p and D_{st} while correlation studies have generally

237 found a very weak relationship.

238 This work presents an analysis of two types of events intended to provide insight into the

239 relationship between ρ_{eq} and solar wind and geomagnetic parameters by considering both

240 large geomagnetic events and large ρ_{eq} events. The two types of events were considered in

241 order to account for a difficulty with the identification of the cause in ρ_{eq} enhancements,

242 which can occur for two reasons: (1) an extended period of positive B_z, which leads to low

243 geomagnetic activity, plasmasphere refilling, and a possible expansion of the plasmasphere to

244 geosynchronous altitudes and (2) strong negative B_z, which (a) leads to the inward motion

245 of the higher density plasmasphere and leaves geosynchronous altitudes in the lower den-

246 sity plasma trough just outside of the plasmapause and (b) causes possible magnetospheric

247 processes to enhance the mass density at geosynchronous altitudes.

248 On average, around the time of large geomagnetic events, there is a statistically weak

249 enhancement of daily-averaged ρ_{eq} measurements. For hourly averages, ρ_{eq} shows enhance-

250 ments over a 6-hour post-onset window that contains too few events for a statistical analysis.

When the constraint of extended geomagnetic events (greater than 12 hours below a threshold value) and the MLT of the observation of ρ_{eq} (06:00-12:00) is removed to allow for more events, statistically significant variations are found, with a peak occurring approximately six hours after the event onset. For the hourly-averaged measurements, ρ_{eq} averages within 7-11 hours after the onset time was lower when the average of B_z four hours after the onset time was more positive. This result highlights the complexity of the response of ρ_{eq} to solar wind driving. Negative values of B_z are generally needed for a large geomagnetic event to occur and we have shown an association between large geomagnetic events and increases in ρ_{eq} within six hours of the event onset, but after the onset of the event, more positive values of B_z are associated with larger ρ_{eq} values.

It was shown that a key factor in determining if large ρ_{eq} enhancements will be observed is elevated $F10.7$. When geomagnetic events were separated according to if they occurred when $F10.7$ was low or high, larger enhancements in ρ_{eq} above a baseline value were only observed under high $F10.7$ conditions.

For ρ_{eq} events, more positive B_z after onset corresponded to higher values of subsequent ρ_{eq}, which indicates that a substantial portion of the events may be due to the apparent mass refilling mechanism described by *Denton et al.* [2016]. In order to separate this mechanism from an enhancement due to magnetospheric activity using this type of analysis, additional information about the location of the plasmapause may be required.

4   Acknowledgements

References

Carpenter, D. L., Whistler studies of the plasmapause in the magnetosphere: 1. Temporal variations in the position of the knee and some evidence on plasma motions near the knee, *J. Geophys. Res.*, *71*, 693–709, 1966.

Carpenter, D. L., and R. R. Anderson, An ISEE/whistler model of equatorial electron density in the magnetosphere, *J. Geophys. Res.*, *97*, 1097–1108, 1992.

Chappell, C. R., K. K. Harris, and G. W. Sharp, A study of the influence of magnetic activity on the location of the plasmapause as measured by OGO 5, *J. Geophys. Res.*, *75*, 50–56, 1970.

Denton, R., Database of Input Parameters for Tsyganenko Magnetic Field Models, 2007.

Denton, R. E., K. Takahashi, I. A. Galkin, P. A. Nsumei, X. Huang, B. W. Reinisch, R. R. Anderson, M. K. Sleeper, and W. J. Hughes, Distribution of density along magnetospheric field lines, *J. of Geophys. Res.*, *111*, 4213, 2006.

Denton, R. E., M. F. Thomsen, K. Takahashi, R. R. Anderson, and H. J. Singer, Solar cycle dependence of bulk ion composition at geosynchronous orbit, *J. Geophys. Res.*, *116*, n/a–n/a, 2011.

Denton, R. E., K. Takahashi, J. Amoh, and H. J. Singer, Mass density at geostationary orbit and apparent mass refilling, *J. Geophys. Res.*, *121*, 2962–2975, 2016.

Gallagher, D. L., P. D. Craven, and R. H. Comfort, An empirical model of the earth's plasmasphere, *Advances in Space Research*, *8*, 15–21, 1988.

Kondrashov, D., R. Denton, Y. Y. Shprits, and H. J. Singer, Reconstruction of gaps in the past history of solar wind parameters, *Geophys. Res. Lett.*, *41*, 2702–2707, 2014.

Lemaire, J., *The Earth's Plasmasphere*, Cambridge University Press, 1998.

Maynard, N. C., and J. M. Grebowsky, The plasmapause revisited, *J. Geophys. Res.*, *82*, 1591–1600, 1977.

Moldwin, M. B., L. Downward, H. K. Rassoul, R. Amin, and R. R. Anderson, A new model of the location of the plasmapause: CRRES results, *J. of Geophys. Res.*, *107*, 1339, 2002.

O'Brien, T. P., and M. B. Moldwin, Empirical plasmapause models from magnetic indices, *Geophys. Res. Lett.*, *30*, 1–1, 2003.

Takahashi, K., R. E. Denton, R. R. Anderson, and W. J. Hughes, Mass density inferred from toroidal wave frequencies and its comparison to electron density, *J. of Geophys. Res.*, *111*, 1201, 2006.

Takahashi, K., R. E. Denton, and H. J. Singer, Solar cycle variation of geosynchronous plasma mass density derived from the frequency of standing Alfvén waves, *J. of Geophys. Res.*, *115*, 7207, 2010.

Yao, Y., K. Seki, Y. Miyoshi, J. P. McFadden, E. J. Lund, and C. W. Carlson, Effect of solar wind variation on low-energy O^+ populations in the magnetosphere during geomagnetic storms: FAST observations, *J. of Geophys. Res.*, *113*, 2008.

₃₁₀ # 5 Figures
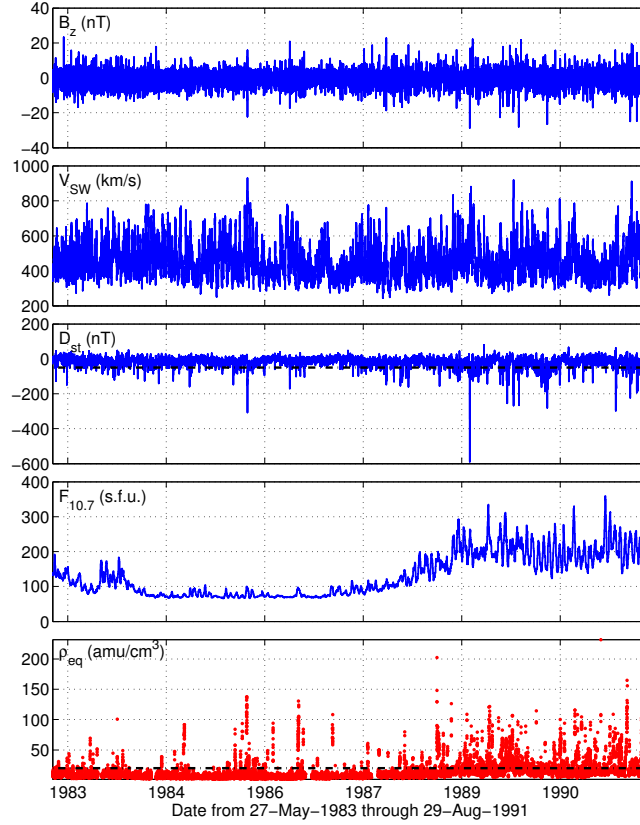
Figure 1: Overview of data used in this article. The top four panels show parameters from *Kondrashov et al.* [2014] and the bottom panel contains ρ_{eq} based on GOES 6 measurements from *Denton* [2007] after interpolation and averaging described in the text. Dashed horizontal lines in the D_{st} and ρ_{eq} panels indicate sample event cutoff thresholds of $D_{st} = -50$ nT and $\rho_{eq} = 20$ amu/cm^3 considered in Section 3.
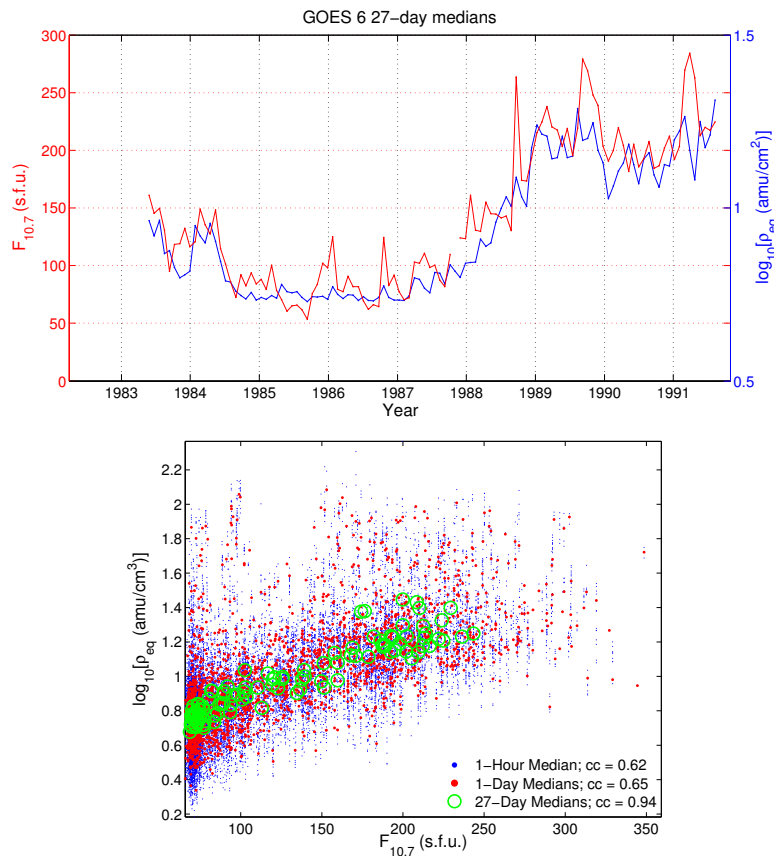
Figure 2: Top: 27-day non-overlapping medians of $F_{10.7}$ and $\log_{10}(\rho_{eq})$ from GOES 6. Bottom: Scatter plot of $\log_{10}(\rho_{eq})$ and $F_{10.7}$ using medians in non-overlapping hour, day, and 27-day windows.
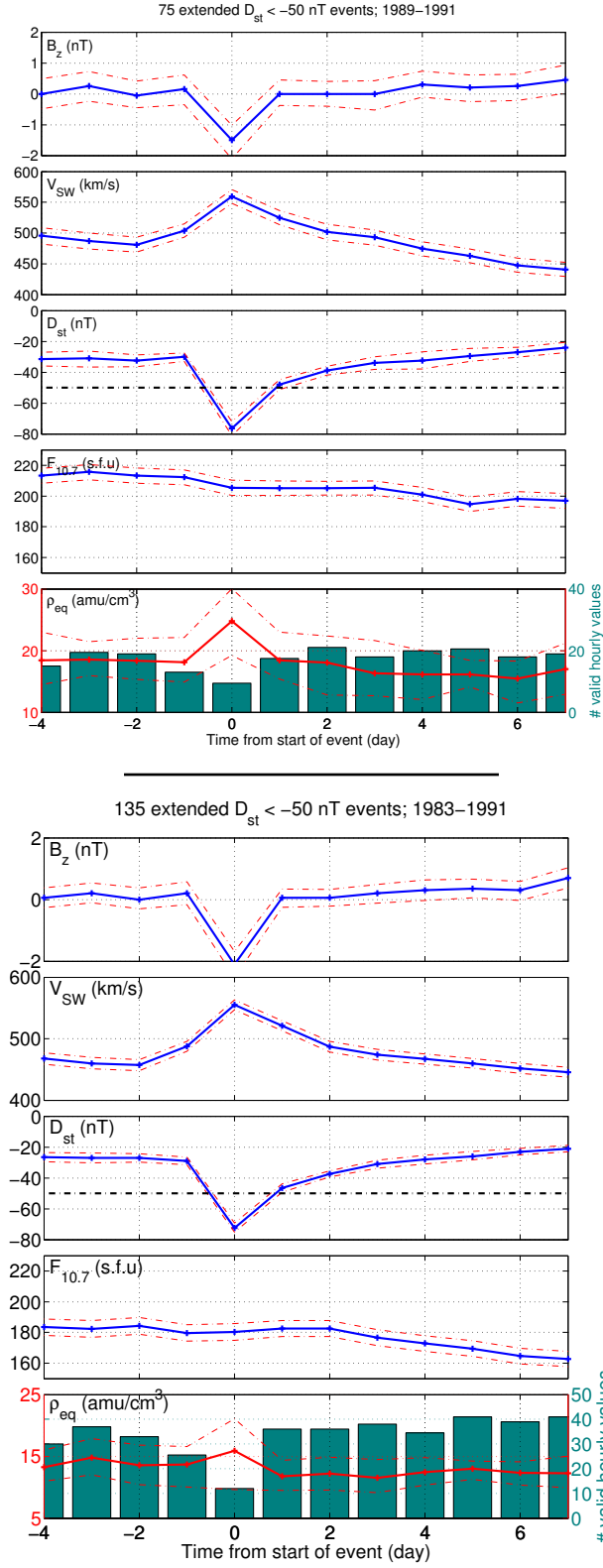
Figure 3: D_{st} events from GOES 6 using daily medians. Top: Events in the interval 1989-1991; compare to *Takahashi et al.* [2010] Figure 11. Bottom: Events in the interval 1983-1991.
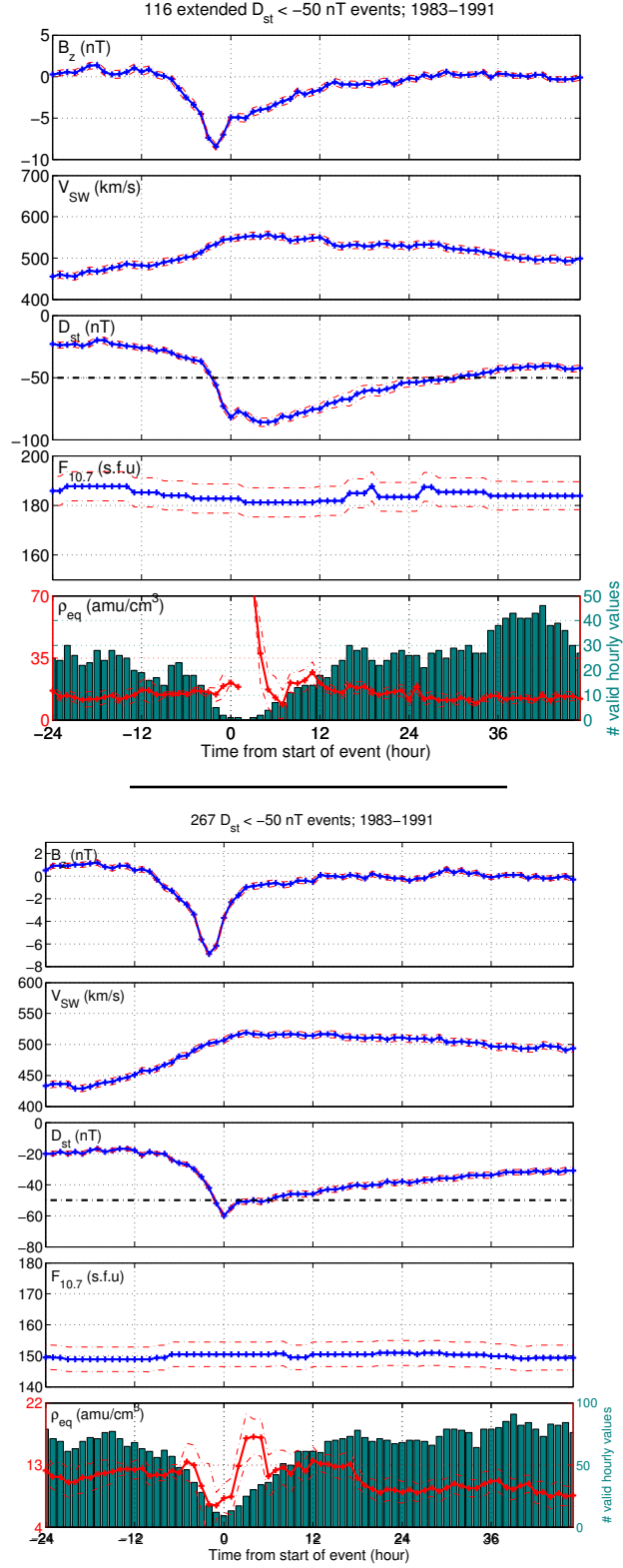
Figure 4: D_{st} events from GOES 6 using hourly medians. Top: Events with the constraint that D_{st} stayed below -50 nT for at least 12 hours after crossing below -50 nT. Bottom: Same as Top except without constraint.
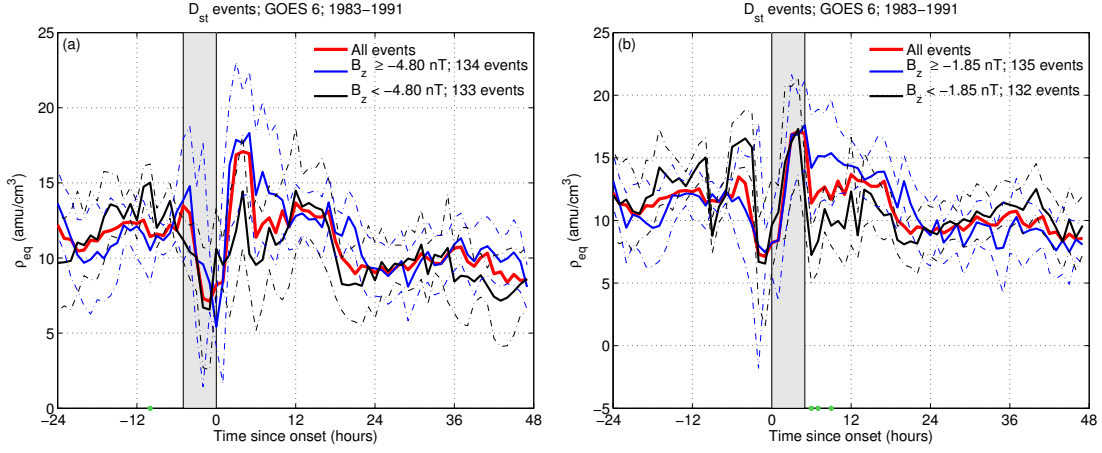
Figure 5: D_{st} events of the bottom panel of Figure 4 separated by the average D_{st} value (a) at onset and four hours before, and (b) at onset and four hours after.
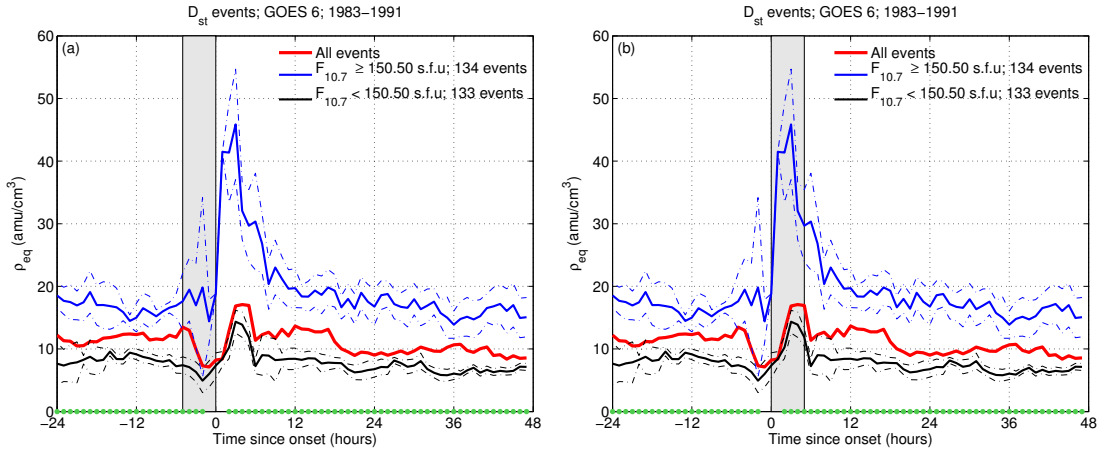
Figure 6: D_{st} events of the bottom panel of Figure 4 separated by the average $F10.7$ value (a) at onset and four hours before, and (b) at onset and four hours after.
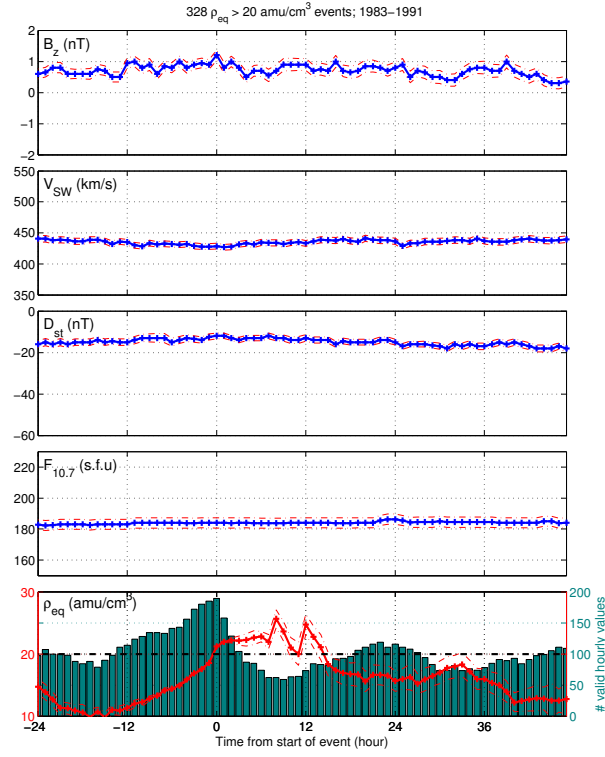
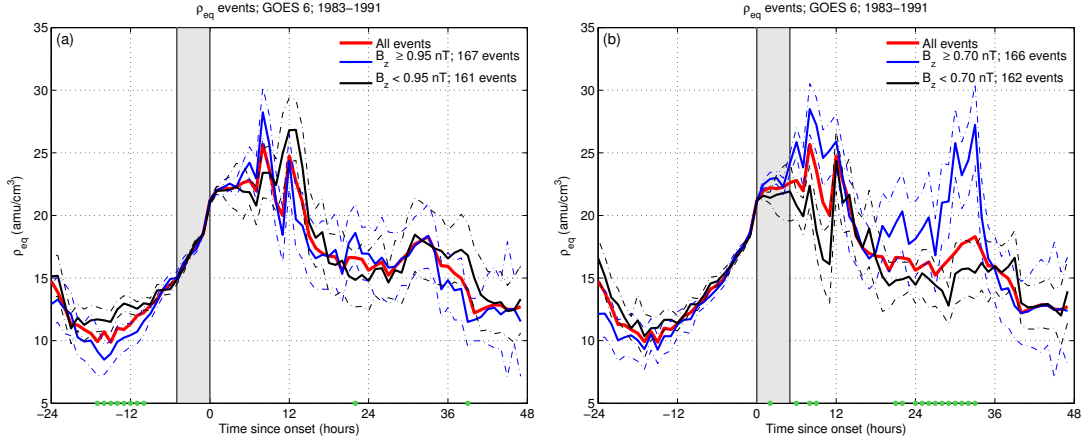Figure 7: $\rho_{eq} > 20$ amu/cm^3 events from GOES 6 using hourly medians.

Figure 8: ρ_{eq} events of Figure 7 separated by the average B_z value (a) at onset and four hours before, and (b) at onset and four hours after.
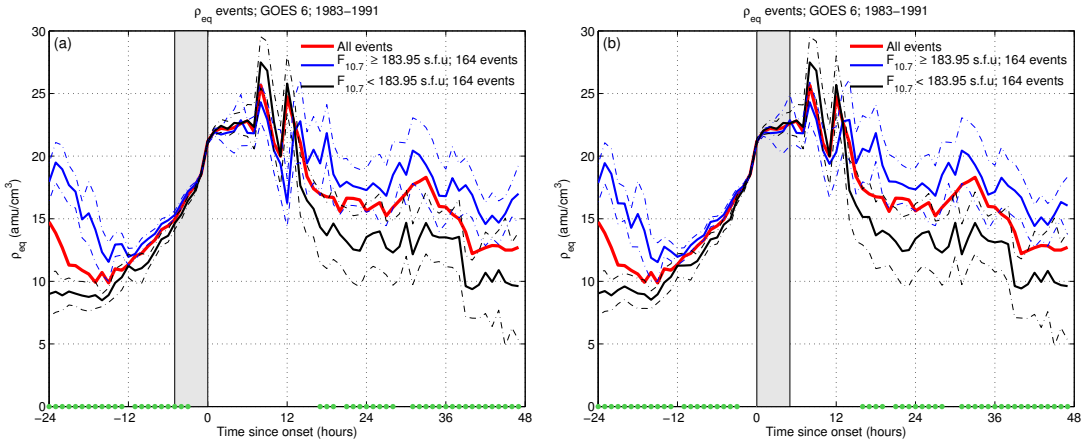

Figure 9: ρ_{eq} events of Figure 7 separated by the average $F10.7$ value (a) at onset and four hours before, and (b) at onset and four hours after.